Surface damage characterization of photodegraded low-density polyethylene by means of friction measurements

著者	Igarashi Toshio, Ohno Soichiro, Oda Sayaka, Hirosawa Satoru, Hiejima Yusuke
著者別表示	比江嶋 祐介
journal or publication title	Journal of Polymer Engineering
volume	39
number	9
page range	805-812
year	2019-10-01
URL	http://doi.org/10.24517/00055783

doi: 10.1515/polyeng-2019-0071

Surface damage characterization of photodegraded low-density polyethylene by means of friction measurements

Toshio Igarashi[1], Soichiro Ohno[1], Sayaka Oda[2], Satoru Hirosawa[2], Yusuke Hiejima[1] and Koh-hei Nitta[1*]

1. Department of Chemical and Materials Science, Kanazawa University, Kakuma Campus, Kanazawa 920-1192, Japan

2. Kyoto Municipal Institute of Industrial Technology and Culture, 91 Awata-cho, Chudoji, Shimogyo-ku, Kyoto 600-8815, Japan

* Corresponding author: nitta@se.kanazawa-u.ac.jp

ORCID IDs

0000-0001-9197-2021 (Yusuke Hiejima)

0000-0002-1218-2935 (Koh-hei Nitta)

Acknowledgment

The authors are thankful to Mr. Y. Yonezawa (Adeka Corp.) and Prof. M. Yamaguchi (Japan Advanced Institute of Science and Technology (JAIST)) for performing the UV exposure tests and the white light interferometric microscope measurements, respectively. This work was financially supported by KAKENHI (grant number 16K14456).

Abstract

Friction measurements have been carried out to characterize surface damages during photodegradation of low-density polyethylene (LDPE). The average and mean deviation of the friction coefficients increase with the irradiation time in the early stage of photodegradation processes, indicating the increase of the surface roughness, whereas the mechanical properties remain essentially unchanged. In the following stage, where the ductile-brittle transition takes place, the mean deviation of the friction coefficients shows an appreciable decrease with maintaining almost constant average values, suggesting that the surface becomes more homogeneous. Beyond the ductile-brittle transition, both of the average and mean deviation of the friction coefficients gradually increase with the irradiation time, indicating further enhancement of surface roughness, followed by formation of surface cracks. The soundness of the friction measurements is confirmed by comparing with optical measurements of the surface roughness, and it is suggested that the present method gives a convenient and sensitive method of detection for degradation in polymeric materials.

Introduction

Polyethylene (PE) has been used ubiquitously in our daily life. Excellent properties of plastics including polymer composites [1-5], such as lightweight and high toughness of plastics promote further replacement from metal and inorganic materials. However, durability has been one of the major concerns of polymeric materials that are prone to be oxidized, resulting in deterioration of appearances and properties. Applications of polymeric materials for long-term use, such as vehicles and constructions urge development of simple methods for non-invasive diagnostics of degradation of polymer products under use.

Degradation of PE can be induced by various environmental factors, such as sunlight, heat, and various dynamic behavior, which result in deterioration of the physical properties, such as the color change, gloss, and impact strength. The mechanism of degradation and deterioration in various environments has also been discussed [6 –15]. These mechanisms of various PE materials have been intensively investigated for films [16-23] and pipes [24-28], and it has been revealed that the degradation proceeds in distinctive stages. The strength of pipes or films gradually decreases in the early stage (hereafter referred as 1st stage), where the fracture becomes ductile. After the 1st stage, the decline of the strength obviously becomes steeper, and the fracture becomes brittle (2nd stage). Then, it is considered that a ductile-brittle transition takes place between the 1st and 2nd stages, and the practical lifetime of the material is terminated. After the 2nd stage, it was found that the strength of polymeric pipe drops, and the brittle fracture occurs at substantially smaller stress (3rd stage). It has been found that chemical degradation is accelerated, and the integrity in the material is lost during the 3rd stage [29-32].

During degradation in the 2nd stage, surface modification of pipes such as stress corrosion cracking and environmental stress cracking is observed [24,33]. It is known that surface roughness measurements

are useful to detect such failures [26]. Several methods of measurements for surface friction of polymeric materials have been established (e.g. ISO 8295) [34-36], though these techniques are not suitable to detect small changes during degradation [37,38]. On the other hands, various techniques have been developed to detect subtle changes in human skins for medical and cosmetic purposes. Benchtop and mobile apparatuses, as well as a variety of probes for frictions during linear and rotational motions, have been developed [39-52]. These techniques developed in skin science have recently applied to various fields, such as sensory test for piles [53] and woods [54].

In this work, friction measurements under two-dimensional linear motion were applied, and the coefficients of friction were determined for photodegraded low-density polyethylene (LDPE) films. The ultraviolet (UV) irradiation time dependence of the coefficients of friction was compared with that of the surface roughness determined by white light coherence microscopy. Effects of degradation on the surface and the bulk properties are described, and detection of the degradation/deterioration processes with the friction measurements is discussed.

Materials and methods

LDPE (Prime Polymer Co., Ltd.) with a density of 0.92 g/cm^3 and a melt-flow index of 4 g/10 min was used. We have confirmed that the LDPE contained 0.2 wt% of dibutylhydroxytoluene as the antioxidant. To simulate the rotational molding process, LDPE sheets with a thickness of 0.5 mm were prepared as follows. The LDPE powder was preheated in a hot press at 150°C for 3 min and then degassed at 150°C for 2 min. The sample was pressurized at 10 MPa for 1 min. The sample was then heated to 200°C in 8 min and gradually cooled to 180°C in 8 min, followed by quenching to room temperature.

The photodegraded LDPE sheets were prepared with a Xenon Weather Meter (SX2-75, Suga Test Instruments, Tokyo, Japan). A Xenon fade lamp was used as the light source. The LDPE sheets were irradiated at 60 W/m^2 in a wavelength range 300–400 nm at a black panel temperature of 89°C under the no rain condition. Note that the present condition has recently been employed for interior components of automobiles, in accordance with increasing demands for harsh conditions such as in the desert area. The irradiation time was set at 120–1200 h. The surface of the photodegraded LDPE specimens was observed with an optical microscope (Digital Microscope VHX-1000, Keyence, Osaka, Japan). The yellowness index of the LDPE specimens was measured with a spectrocolorimeter (SC-T(P), Suga Test Instruments, Tokyo, Japan) in a range of wavelength from 380 to 780 nm. The gloss value of the LDPE specimens was measured with a gloss meter (VG-2000, Nippon denshoku industries, Tokyo, Japan) at an angle of 60°. High-temperature gel permeation chromatography (HT-GPC) was performed at 140 °C using a Viscotek Triple Detector HT-GPC (Model- SG system, Malvern Instruments Ltd., Worcestershire, UK). The samples were dissolved into *o*-dichlorobenzene at 140 °C to obtain a concentration of 1.0 mg/ml. A polystyrene standard sample was used for column calibration. The DSC measurements were performed with a PerkinElmer Diamond differential scanning calorimeter from 25 to 230 °C at a rate of 20 °C/ min in a nitrogen atmosphere. Dynamic mechanical analysis (DMA) was carried out by using a dynamic mechanical analyzer (DVE-4, UBM, Kyoto, Japan) with a rectangular specimen (5 mm ×30 mm). The LDPE samples were sputter-coated with Au-Pt alloy in vacuum, and the surface of the samples was observed by scanning electron microscope (S-4500, Hitachi, Tokyo, Japan) at a voltage of 2.0 kV.

Surface friction of the LDPE sheets was measured with a friction evaluation meter (TL-201Ts, Trinity Lab, Tokyo, Japan). The LDPE specimen was fixed on a horizontal stage. A hemispherical metal probe with a diameter of 8.0 mm was pressed onto the surface of the LDPE specimen at a constant load of

2.9 N as the normal force N. The horizontal stage was swept at a rate of 0.1 mm/s for 20 mm, and the frictional force F was monitored in a time resolution of 10 ms. The measurements were repeated for three times. The friction coefficient x_i (i=1, 2, ... , n) at each point was determined by the Amontons-Coulomb friction law

$$F = x_i N \tag{1}$$

The average value $\bar{x}$ and mean deviation $\overline{\Delta x}$ of the friction coefficients were calculated by

$$\bar{x} = \frac{1}{n}\sum_{i=1}^{n} x_i \tag{2}$$

and

$$\overline{\Delta x} = \frac{1}{n}\sum_{i=1}^{n}\left|x_i - \bar{x}\right| \ , \tag{3}$$

respectively.

Surface height profile was measured with a white light interferometric microscope (BW-S506, Nikon, Tokyo, Japan) [55-57]. The surface of the sample in 1 mm length within ±20 μm height was scanned at every 20 nm for three times. The average roughness R_a was determined from the surface profile $f(x)$ as

$$R_a = \frac{1}{L}\int_0^L \left|f(x) - f_0\right| dx \ , \tag{4}$$

where f_0 is the average height and L =1 mm is the scanned length.

Results and discussion

Optical microscopic images of the photodegraded LDPE are shown in Fig. 1(a). The surface of the LDPE specimens is smooth before irradiation but the surface cracks have propagated over the entire surface after the UV irradiation for 1080 h. The initiation of the crack formation was observed at 840 and

960 h, as denoted by the circles. The formation of surface cracks along with enhancement of surface roughness are also observed by the SEM images in Fig. 1(b).

As shown in Fig. 2(a), the yellowness index gradually decreases with the UV irradiation time, followed by a rise after 480 h. The molecular weight of LDPE shows obvious decrease at 600 h as shown in Fig. 2(b). Considering that the molecular weight shows appreciable decrease after 600 h, the increase of the yellowness index is likely to be caused by the increase of conjugated double bonds owing to the chain scission.

The profiles of the friction coefficient for the photodegraded LDPE at various UV irradiation times are shown in Fig. 3. While the fluctuation of the friction coefficient is small before the UV irradiation, the fluctuation becomes enhanced with increasing the irradiation time. In the early stage from 120 to 360 h, fluctuation of the friction coefficient is observed locally. Then, the small fluctuation appears to spread in the whole range from 480 to 720 h. Finally, the fluctuation becomes markedly large after 960 h. The average and mean deviation of the friction coefficient calculated by Eqns. (2) and (3) are plotted against the irradiation time in Fig. 4. The average value $\bar{x}$ gradually increases with increasing the irradiation time up to about 360 h, followed by a plateau at 360-600 h. After 600 h, $\bar{x}$ resumes increasing up to 960 h again, followed by an appreciable drop at 1080 h. The mean deviation $\overline{\Delta x}$ also shows similar irradiation time dependence; $\overline{\Delta x}$ gradually increases with the irradiation time in the initial stage, and shows a maximum around 360 h. After 600 h, $\overline{\Delta x}$ also increases with the irradiation time. Then, the degradation process seems to be divided into three regions. In the 1st (0-360 h) and 2nd (600-960 h) stages, both of $\bar{x}$ and $\overline{\Delta x}$ gradually increases with the irradiation time, suggesting monotonous increase of the surface roughness. In the transition stage (360-600 h), $\bar{x}$ shows a plateau, whereas $\overline{\Delta x}$ shows appreciable decrease, suggesting that the surface becomes more homogeneous. It is noteworthy

that the error bar at 360 h is substantially large, suggesting that the inhomogeneity in the surface roughness shows a maximum at the beginning of the transition stage. Since the early stage of oxidation in sold polymer is somewhat localized [6], it is suggested that the present measurement is sensitive to inhomogeneity on the surface during photodegradation by detecting as the standard deviation of the friction coefficient. In the 3rd stage (>960 h), $\overline{x}$ shows appreciable drops, while $\overline{\Delta x}$ remains high. Then, the surface roughness is highly enhanced. The large fluctuation in the friction data is explained by the slippage of the probe tips owing to highly-enhanced rough surface accompanied by macroscopic cracks (see Fig. 1).

The surface height profiles $f(x)$ of the photodegraded LDPE specimens are shown in Fig. 5. While the profile is practically flat before irradiation, the fluctuation in the surface profile increases with the irradiation time. The temporal changes of the surface profiles are consistent with the friction measurements; formation of local fluctuation at 120-360 h is followed by homogeneous fluctuation at 480-720 h and enhanced roughening after 840 h. The average roughness R_a calculated by Eq. (4) is shown in Fig. 6. The value of R_a linearly increases with the irradiation time, and shows a plateau at 360-600 h, followed by gradual increase after 720 h. The correlation between R_a and $\overline{x}$ is shown in Fig. 7. These quantities show excellent linear correlation from 240 to 960 h, indicating that the present friction measurements successfully probe the surface roughness of the photodegraded LDPE specimens. The initial deviation before 240 h results from that the surface roughness is too small to detect the present probe. The lower deviation of $\overline{x}$ after 1080 h is considered to be caused by the slip of the probe tip owing to the macroscopic surface crack.

Dynamic mechanical spectra of photodegraded LDPE after the UV exposure tests are shown in Fig. 8(a). It is noteworthy that the photodegraded specimens with irradiation time longer than 720 h are too

brittle to perform the mechanical test. The β relaxation peak at around -20°C is assigned to the glass transition. The peak position of the β relaxation obviously shifts toward higher temperature after 480 h, indicating a rise in the glass transition temperature T_g as shown in Fig. 8(b). The higher temperature shift of the glass transition is explained as the stiffening of amorphous chains [58], reminding us of rigid amorphous chains. The DMA results indicate that the mechanical properties of bulk LDPE are appreciably deteriorated in the 2nd stage, because the degradation due to the reduction of molecular weight and/or yellowing spread over the entire body of the specimen. In fact, we have confirmed the overall crystallinity of the LDPE specimens sharply increases at around 600 h. Then, it is reasonable that surface characterization by the friction measurement can detect subtle changes in the earlier stage, before the bulk mechanical properties are deteriorated. The DSC traces of the photodegraded LDPE are shown in Fig. 9. A hump at 90-110°C is observed during heating of LDPE after the UV exposure tests. These humps which disappear in the second run are explained by the thermal history during the UV exposure tests. Then, the slight lower shift of T_g at 120 h is explained by the softening of the amorphous chains owing to the annealing effect. Slight shift of the crystallization peak toward higher temperature along with evolution of another peak at higher temperature after 600 h is consistent with the drop of the molecular weight, leading to promotion of crystallization due to shorter chains formed by the chain scission.

The present results of the friction measurements are consistent with the changes in the gloss values. The irradiation time dependence of the gloss is shown in Fig. 10. The gloss gradually decreases with the irradiation time, followed by a steeper slope after 360 h. Considering that the surface roughness shows a plateau at 360-600 h in Fig. 4 and 6, the accelerated loss of gloss may be caused by microstructural changes in the bulk LDPE specimen owing to penetration of degradation reaction. In fact, the increase of

the glass transition temperature is obvious after 360 h.

Conclusion

The friction measurements have successfully applied to detect three distinctive stages during photodegradation of LDPE. In the 1st stage, surface roughness gradually increases with the UV irradiation time, while conventional methods such as the yellowness index and the gloss are not sensitive to the subtle changes. Moreover, the mechanical properties of the specimens are also essentially unchanged. It was found that the surface of the specimen becomes more homogeneous during ductile-brittle transition. The glass transition temperature of the amorphous region shows appreciable increase, resulting in the stiffening of the material. In the 2nd stage, the various degradation phenomena are observed, such as a rapid increase in yellowing index and a sharp drop in gloss value. In the following 3rd stage, formation of surface cracks leads to loss of integrity and fragmentation into small pieces (e.g. microplastics [59]). It was demonstrated that the friction measurement is sufficiently sensitive to detect subtle changes in the surface roughness. Because handheld apparatus is available for friction measurements, the present method makes it possible to provide a facile and non-destructive method for charactering the degradation in polymeric materials under use.

Reference

1. Yang X, Tang L, Guo Y, Liang, C, Zhang, Q, Kou K, Gu J (2017) Improvement of thermal conductivities for PPS dielectric nanocomposites via incorporating NH2-POSS functionalized nBN fillers. Composites A 101: 237-242. http://dx.doi.org/10.1016/j.compositesa.2017.06.005
2. Gu J, Li N, Tian L, Lv Z, Zhang Q (2015) High thermal conductivity graphite nanoplatelet/ UHMWPE nanocomposites. RSC Advances 5: 36334-36339. doi: 10.1039/C5RA03284A
3. Gu J, Guo Y, Lv Z, Geng W, Zhang Q (2015) Highly thermally conductive POSS-g-SiCp/UHMWPE composites with excellent dielectric properties and thermal stabilities. Composites A 78: 95-101. http://dx.doi.org/10.1016/j.compositesa.2015.08.004
4. Gu J, Zhang Q, Dang J, Zhang J, Yang Z (2009) Thermal Conductivity and Mechanical Properties of Aluminum Nitride Filled Linear Low-Density Polyethylene Composites. Polym Eng Sci 49: 1030-1034 doi: 10.1002/pen.21336
5. Gu JW, Zhang Q, Zhang J, Wang W (2010) Studies on the Preparation of Polystyrene Thermal Conductivity Composites. Polym Plastics Tech Eng 49: 1385-1389 https://doi.org/10.1080/03602559.2010.512326
6. Hamid SH (2000) Handbook of Polymer Degradation, Second edition, Marcel Dekker, New York.
7. Rivaton A, Gardette JL, Mailhot B, Therlas SM (2005) Basic aspects of polymer degradation. Macromol Symp 225: 129-146. https://doi.org/10.1002/masy.200550711
8. Celina M, Gillen KT, Assink RA (2005) Accelerated aging and lifetime prediction: Review of non-Arrhenius behaviour due to two competing processes. Polym Degrad Stab 90: 395-404. https://doi.org/10.1016/j.polymdegradstab.2005.05.004
9. White JR (2006) Polymer ageing: physics, chemistry or engineering? Time to reflect. Compt Rend

Chem 9: 1396-1408. https://doi.org/10.1016/j.crci.2006.07.008

10. Fayolle B, Colin X, Audouin L, Verdu J (2007) Mechanism of degradation induced embrittlement in polyethylene. Polym Degrad Stab 92: 231-238. https://doi.org/10.1016/j.polymdegradstab.2006.11.012

11. Fayolle B, Richaud E, Colin X, Verdu J (2008) Review: degradation-induced embrittlement in semi-crystalline polymers having their amorphous phase in rubbery state. J Mater Sci 43: 6999-7012. https://doi.org/10.1007/s10853-008-3005-3

12. Celina M (2013) Review of polymer oxidation and its relationship with materials performance and lifetime prediction. Polym Degrad Stab 98: 2419-2429. https://doi.org/10.1016/j.polymdegradstab.2013.06.024

13. Singh B (2008) Mechanical implications of plastic degradation. Polym Degrad Stab 93: 561-584. https://doi.org/10.1016/j.polymdegradstab.2007.11.008

14. Sanchez JJ, Navarro MA, Muller AJ, Santana OO (2007) Fracture behavior of medium density polyethylenes by essential work of fracture (EWF). Proc SPE ANTEC 1818-1822.

15. Murzakonova MM, Borukaev TA, Begretov MM, Mikitaev AK (2018) The degradation of polyethylene and mechanisms of its stabilization by azomethinephenylmelamine compounds. Int Polym Sci Tech 41: 43-48. https://doi.org/10.1177/0307174X1404101110

16. Gauthier E, Laycock B, Cuoq FJJM, Halley PJ, George KA (2013) Correlation between chain microstructural changes and embrittlement. Polym Degrad Stab 98: 425-435. https://doi.org/10.1016/j.polymdegradstab.2012.08.021

17. Hsu YC, Truss RW, Laycock B, Weir MP, Nicholson TM, Garvey CJ, Halley PJ (2017) The effect of comonomer concentration and distribution on the photo-oxidative degradation of linear low density

polyethylene films. Polymer 119: 66-75. https://doi.org/10.1016/j.polymer.2017.05.020

18. Hsu YC, Weir MP, Truss RW, Garvey CJ, Nicholson TM, Halley PJ (2012) A fundamental study on photo-oxidative degradation of linear low density polyethylene films at embrittlement. Polymer 53: 2385-2393. https:// doi.org/10.1016/j.polymer.2012.03.044

19. Liu M, Horrocks AR, Hall ME (1995) Correlation of physicochemical changes in UV-exposed low density polyethylene films containing various UV stabilisers. Polym Degrad Stab 49: 151-161. http://dx.doi.org/10.1016/0141-3910(95) 00036-L

20. Briassoulis D, Aristopoulou A, Bonora M, Verlodt I (2004) Degradation characterization of agricultural low-density polyethylene films. Biosyst Eng 88: 131-143. http://dx.doi.org/10.1016/j.biosystemseng.2004.02.010

21. Dilara PA, Briassoulis D (2000) Degradation and stabilization of low-density polyethylene films used as greenhouse covering materials. J Agric Eng Res 76: 309-321. http://dx.doi.org/10.1006/jaer.1999.0513

22. Dilara PA, Briassoulis D (1998) Standard testing methods for mechanical properties and degradation of low density polyethylene (LDPE) films used as greenhouse covering materials: a critical evaluation. Polym Test 17: 549-585. http://dx.doi.org/10.1016/S0142-9418(97)00074-3

23. Cheneler D, Bowen J (2013) Degradation of polymer films. Soft Matter 9: 344-358. http://dx.doi.org/ 10.1039/C2SM26502H

24. Chudnovsky A, Choi BH (2010) Crack initiation in high density polyethylene pipe resulting from chemical degradation. Proc 11th Pan-American Congress of Applied Mechanics.

25. Jassim KA, Jassim WH, Madhi SH (2017) The effect of sunlight on medium density polyethylene water pipes. Energy Procedia 119: 650-655. https://doi.org/10.1016/j.egypro.2017.07.091

26. Ghabeche W, Alimi L, Chaoui K (2015) Degradation of plastic pipe surfaces in contact with an aggressive acidic environment. Energy Procedia 74: 351-364. https://doi.org/10.1016/j.egypro.2015.07.625

27. Wong RX, KhanN, Wu R (2017) Investigation of root cause of polyethylene pipe leaks and bursts. CEED Seminar Proc 85: 85-90.

28. Kowalska B, Klepka T, Kowalski D (2016) Influence of chlorinated water on mechanical properties of polyethylene and polyvinyl chloride pipes. WIT Trans Built Environ 165: 63-74. http://dx.doi.org/10.2495/UW160061

29. Kanters MJW, Remerie K, Govaert LE (2016) A new protocol for accelerated screening of long-term plasticity-controlled failure of polyethylene pipe grades. Polym Eng Sci 56: 676-688. https://doi.org/10.1002/pen.24294

30. Chudnovsky A, Zhou Z, Zhang H, Sehanobish K (2012) Lifetime assessment of engineering thermoplastics. Int J Eng Sci 59: 108-139. https://doi.org/10.1016/j.ijengsci.2012.03.016

31. Gedde UW, Viebke J, Leijstrom H, Ifwarson M (1994) Long-term properties of hot-water polyolefin pipes - a review. Polym Eng Sci 34: 1773-1787. https://doi.org/10.1002/pen.760342402

32. Lang RW, Stern A, Doerner G (1997) Applicability and limitations of current lifetime prediction models for thermoplastics pipes under internal pressure. Angew Makromol Chem 247: 131-145. https://doi.org/10.1002/apmc.1997.052470109

33. Lustiger A, Markham RL (1983) Importance of tie molecules in preventing polyethylene fracture under long-term loading conditions. Polymer 24: 1647-1654. https://doi.org/10.1016/0032-3861(83)90187-8

34. Wrobel G, Szymiczek M (2008) Influence of temperature on friction coefficient of low density

polyethylene. J Achiev Mater Manuf Eng 28: 31-34.

35. Baena JC, Wu J, Peng Z (2015) Wear Performance of UHMWPE and Reinforced UHMWPE Composites in Arthroplasty Applications: A Review. Lubricants 3: 413-436. https://doi.org/10.3390/lubricants3020413

36. Amiri M, Khonsari MM (2010) On the thermodynamics of friction and wear - A Review. Entropy 12: 1021-1049. http://dx.doi.org/ 10.3390/e12051021

37. Egawa M, Oguri M, Hirao T, Takahashi M, Miyakawa M (2002) The evaluation of skin friction using a frictional feel analyzer. Skin Res Tech 8: 41-51. https://doi.org/10.1034/j.1600-0846.2002.080107.x

38. Kuramitsu K, Nomura T, Nomura S, Maeno T, Nonomura Y (2013) Frictional evaluation system with a human finger model. Chem Lett 42: 284-285. https://doi.org/10.1246/cl.2013.284

39. Sivamani RKR, Goodman J, Gitis NV, Maibach HI (2003) Coefficient of friction: tribological studies in man - an overview. Skin Res Tech 9: 227-234. https://doi.org/10.1034/j.1600-0846.2003.02366.x

40. Naylor PFD (1955) The skin surface and friction. Br J Dermatol 67: 239-248. https://doi.org/10.1111/j.1365-2133.1955.tb12729.x

41. El-Shimi AF (1977) In vivo skin friction measurements. Soc Cosmet Chem 28: 37-52.

42. Comaish S, Bottoms E (1971) The skin and friction: deviations from Amonton's laws, and the effects in hydration and lubrication. Br J Dermatol 84: 37-43. https://doi.org/10.1111/j.1365-2133.1971.tb14194.x

43. Koudine AA, Barquins M, Anthoine PH, Auberst L, Leveque JH (2000) Frictional properties of skin: proposal of a new approach. Int J Cosmetic Sci 22: 11-20.

https://doi.org/10.1046/j.1467-2494.2000.00006.x

44. Highley DR, Coomey M, DenBeste M, Wolfram LJ (1977) Frictional properties of skin. J Invest Dermatol 69: 303-305. https://doi.org/10.1111/1523-1747.ep12507530

45. Comaish JS, Harborow PRH, Hofman DA (1973) A hand-held friction meter. Br J Dermatol 89: 33-35. https://doi.org/10.1111/j.1365-2133.1973.tb01914.x

46. Prall JK (1973) Instrumental evaluation of the effect of cosmetic products on skin surfaces with particular references to smoothness. J Soc Cosmet Chem, 24: 693-707.

47. Cua A, Wilheim KP, Maibach HI (1990) Frictional properties of human skin: relation to age, sex and anatomical region, stratum corneum hydration and transepidermal water loss. Br J Dermatol 123: 437-479. https://doi.org/10.1111/j.1365-2133.1990.tb01452.x

48. Asserin J, Zahouani H, Humbert PH, Couturaud V, Mougin D (2000) Measurement of the friction coefficient of the human skin in vivo, Quantification of the cutaneous smoothness. Colloid Surf B Biointerfaces 19: 1-12. https://doi.org/10.1016/S0927-7765(99)00169-1

49. Eisner P, Wilhelm D, Maibach HI (1990) Frictional Properties of Human Forearm and Vulvar Skin: Influence of Age and Correlation with Transepidermal Water Loss and Capacitance. Dermatologica 181: 88-91. https://doi.org/10.1159/000247892

50. Sulzberger MB, Cortese Jr. TA, Fishman L, Wiley HS (1966) Studies on blisters produced by friction I. Results of linear rubbing and twisting technics. J Invest Dermatol 47: 456-465. https://doi.org/10.1038/jid.1966.169

51. Nacht S, Close J, Yeung D, Gans EH (1981) Skin friction coefficient: changes induced by skin hydration and emollient application and correlation with perceived skin feel. J Soc Cosmet Chem 32: 55-65.

52. Hills RJ, Unsworth A, Ive FA (1994) Comparative study of the frictional properties of emollient bath additives using porcine skin. Br J Dermatol 130: 37-41. https://doi.org/10.1111/j.1365-2133.1994.tb06879.x

53. Fujimoto T, Sunderland MR, Tandon SK, Asano CM, Asano A, Murata C, Fukuyama H (2008) Measurement of surface properties using a special sensor developed for pile material. Ind J Fiber Textile Res 33: 253-257.

54. Karana E (2012) Characterization of 'natural' and 'high-quality' materials to improve perception of bio-plastics. J Clean Prod 37: 316-325. https://doi.org/10.1016/j.jclepro.2012.07.034

55. Deck L, de Groot P (1994) High-speed noncontact profiler based on scanning white-light interferometry. Appl Opt 33: 7334-7338. https://doi.org/10.1364/AO.33.007334

56. Matthew H, Vass DG, Begbie ML (1998) Fast surface profiling by spectral analysis of white-light interferograms with Fourier transform spectroscopy. Appl Opt 37: 1764-1769. https://doi.org/10.1364/AO.37.001764

57. Vo Q, Fang F, Zhang X, Gao H (2017) Surface recovery algorithm in white light interferometry based on combined white light phase shifting and fast Fourier transform algorithms. Appl Opt 56: 8174-8185. https://doi.org/10.1364/AO.56.008174

58. Hiejima Y, Kida T, Takeda K, Igarashi T, Nitta KH (2018) Microscopic structural changes during photodegradation of low-density polyethylene detected by Raman spectroscopy. Polym Degrad Stab 150: 67-72 (2018). https://doi.org/10.1016/j.polymdegradstab.2018.02.010

59. Andrady AL (2011) Microplastics in the marine environment. Mar Pollut Bull 62: 1596-1605. https://doi.org/10.1016/j.marpolbul.2011.05.030

(A)

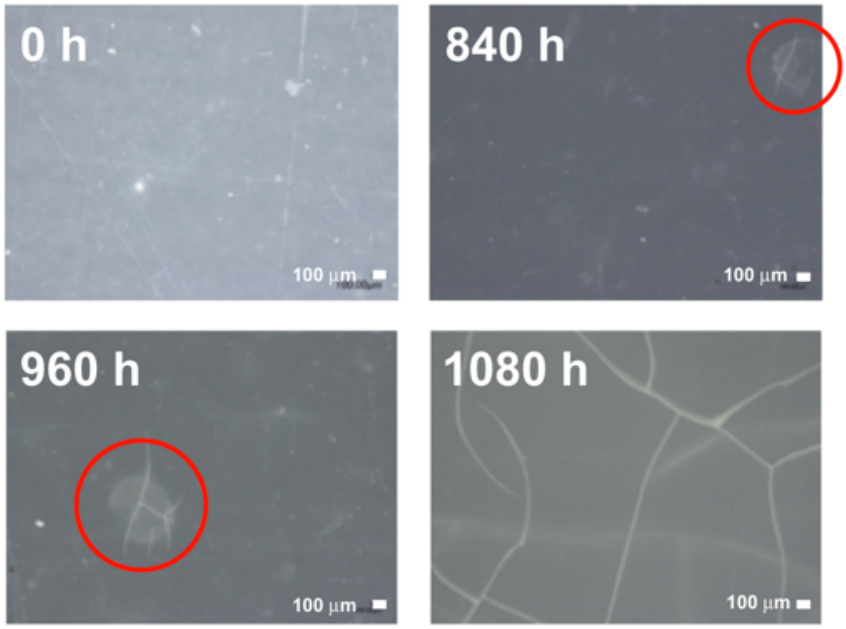

(B)

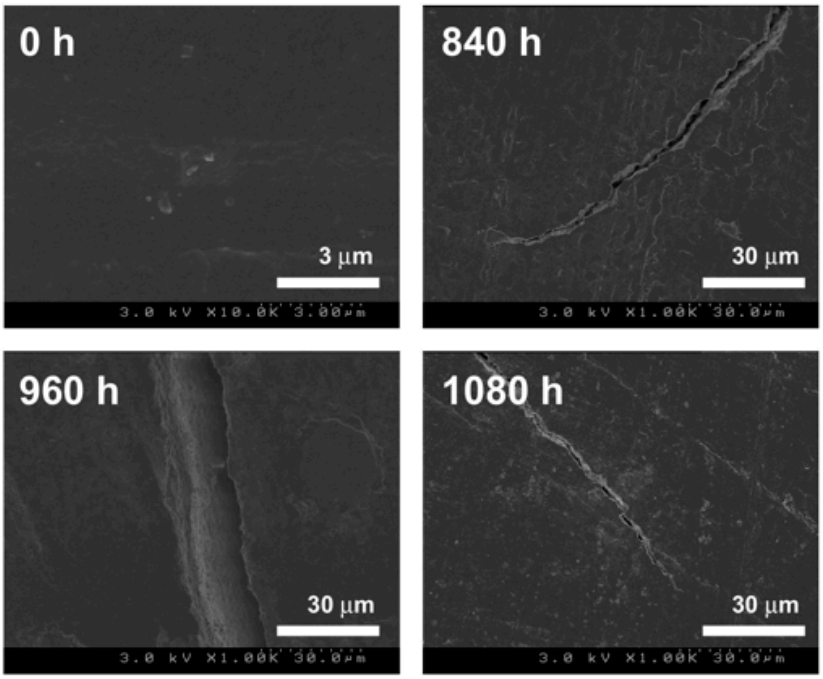

Figure 1 (A) Optical microscopic and (B) SEM images of LDPE specimens after UV irradiation. The UV irradiation times are shown in the figure.

(A)

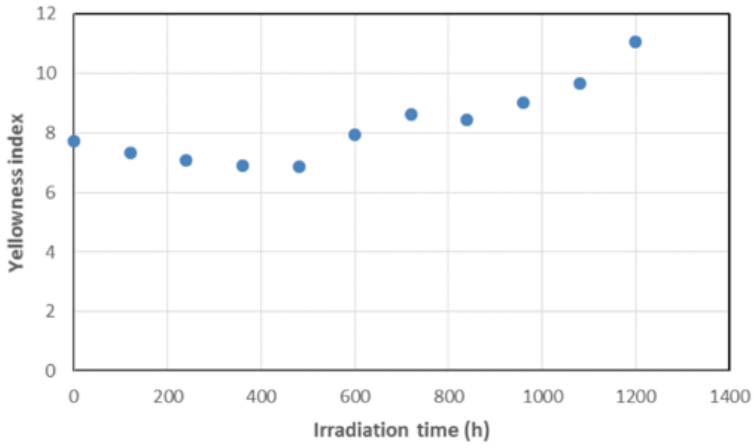

(B)

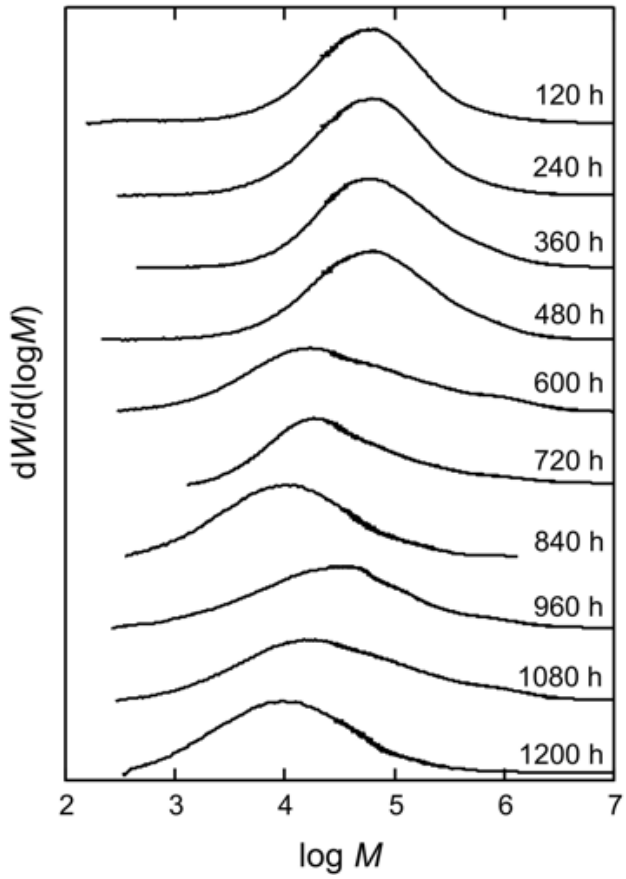

Figure 2 (A) Yellowness index plotted against the UV irradiation time. (B) GPC traces photodegraded LDPE. The UV exposure times are shown in the figure.

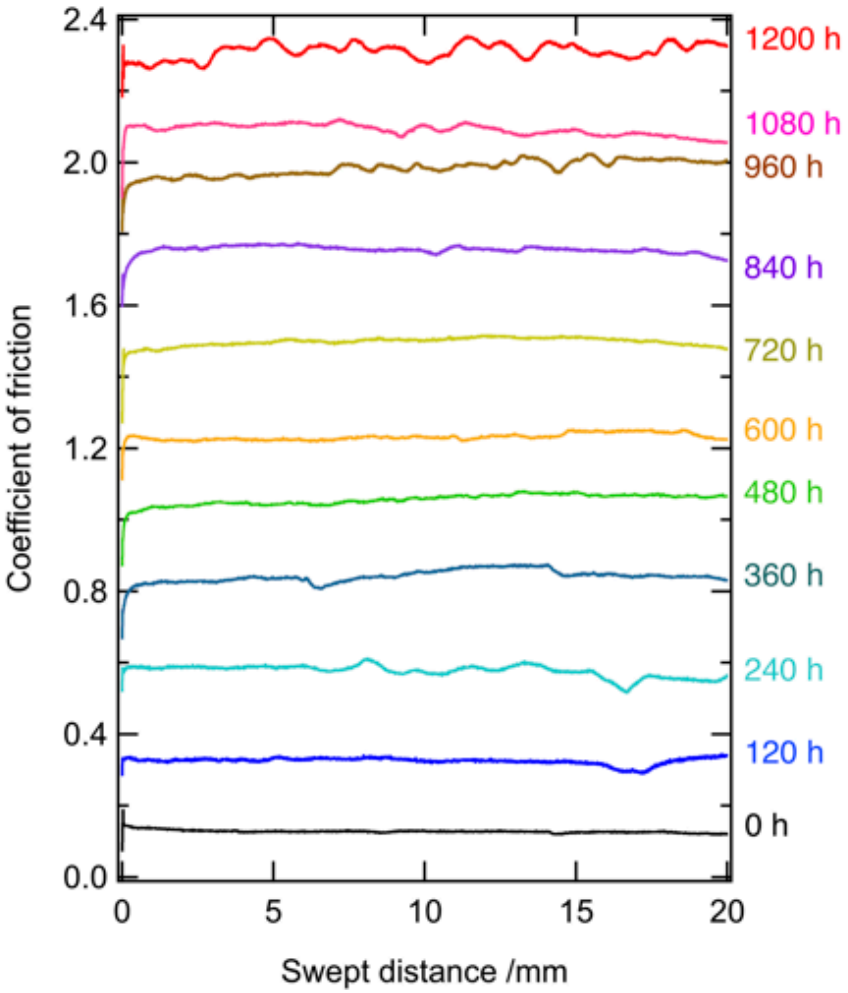

Figure 3 Profiles of friction coefficient for the photodegraded LDPE specimens. The UV irradiation times are shown in the figure. Each profile is vertically shifted by 0.2.

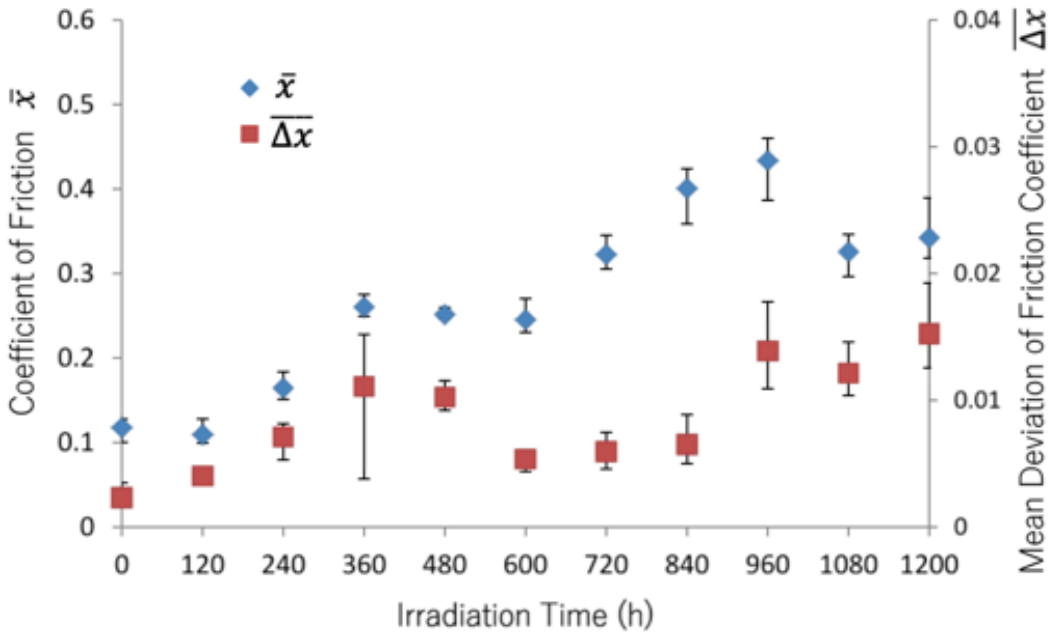

Figure 4 The average value $\bar{x}$ and mean deviation $\overline{\Delta x}$ of the friction coefficient plotted against the UV irradiation time.

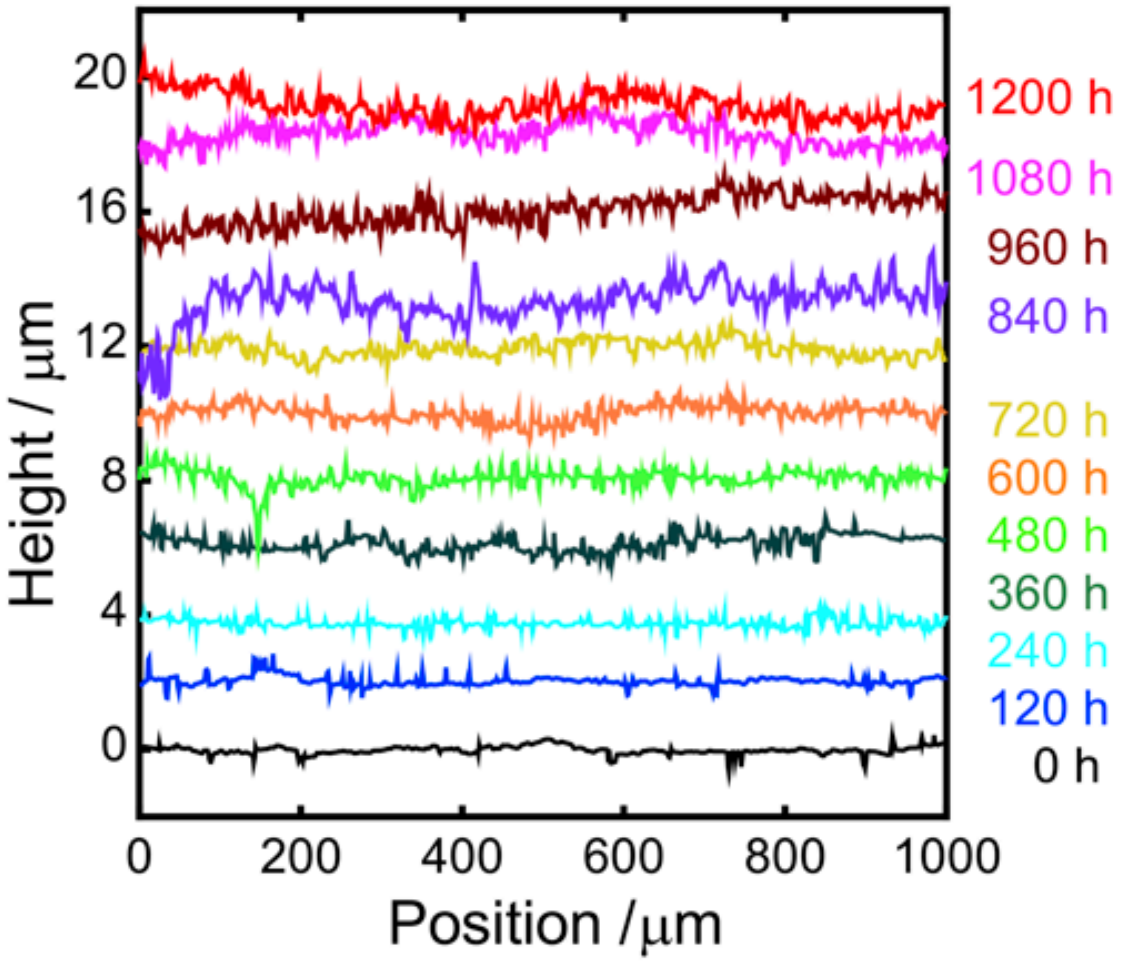

Figure 5 Height profiles of the photodegraded LDPE specimens. Each profile is vertically shifted by 2 μm, and the UV irradiation time is attached.

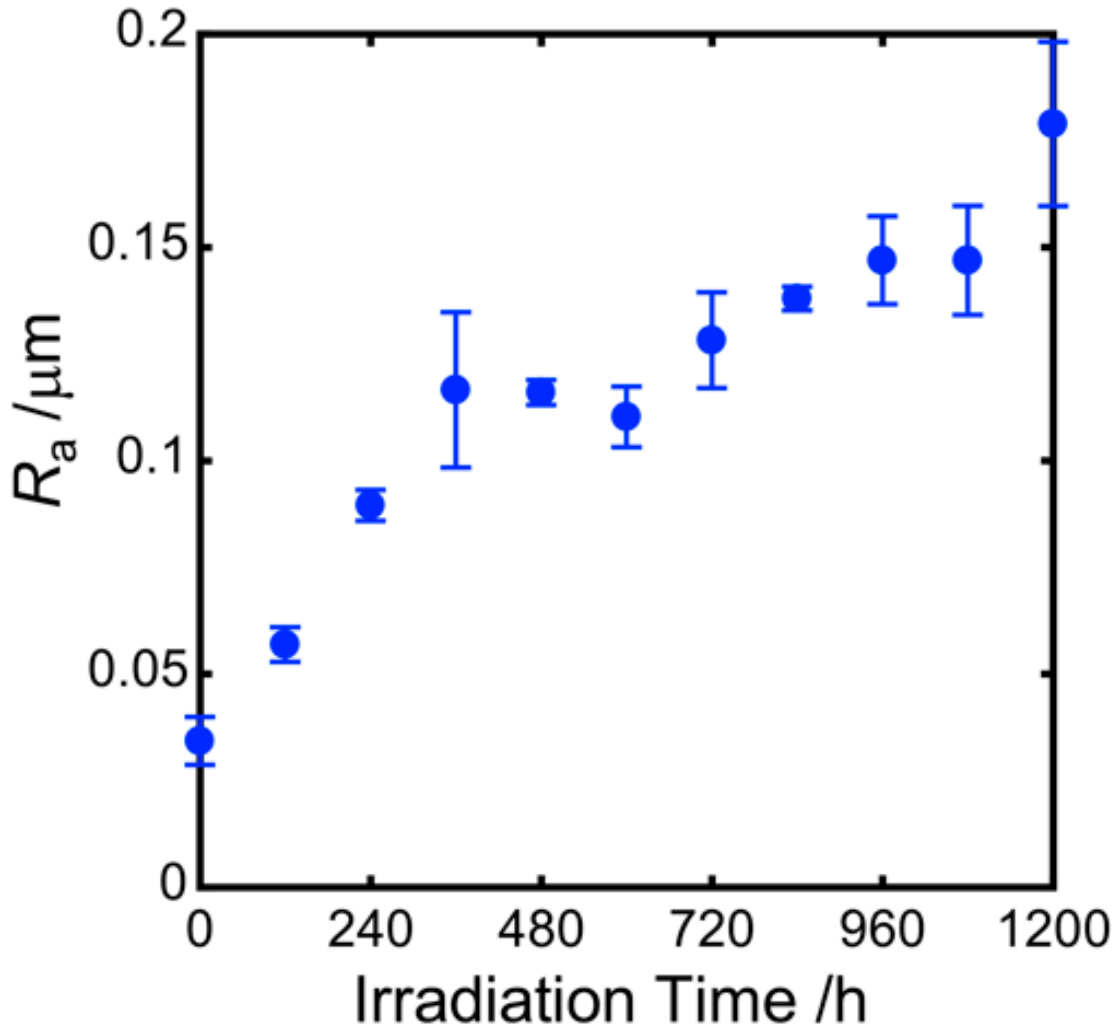

Figure 6 The average roughness R_a as a function of the UV irradiation time.

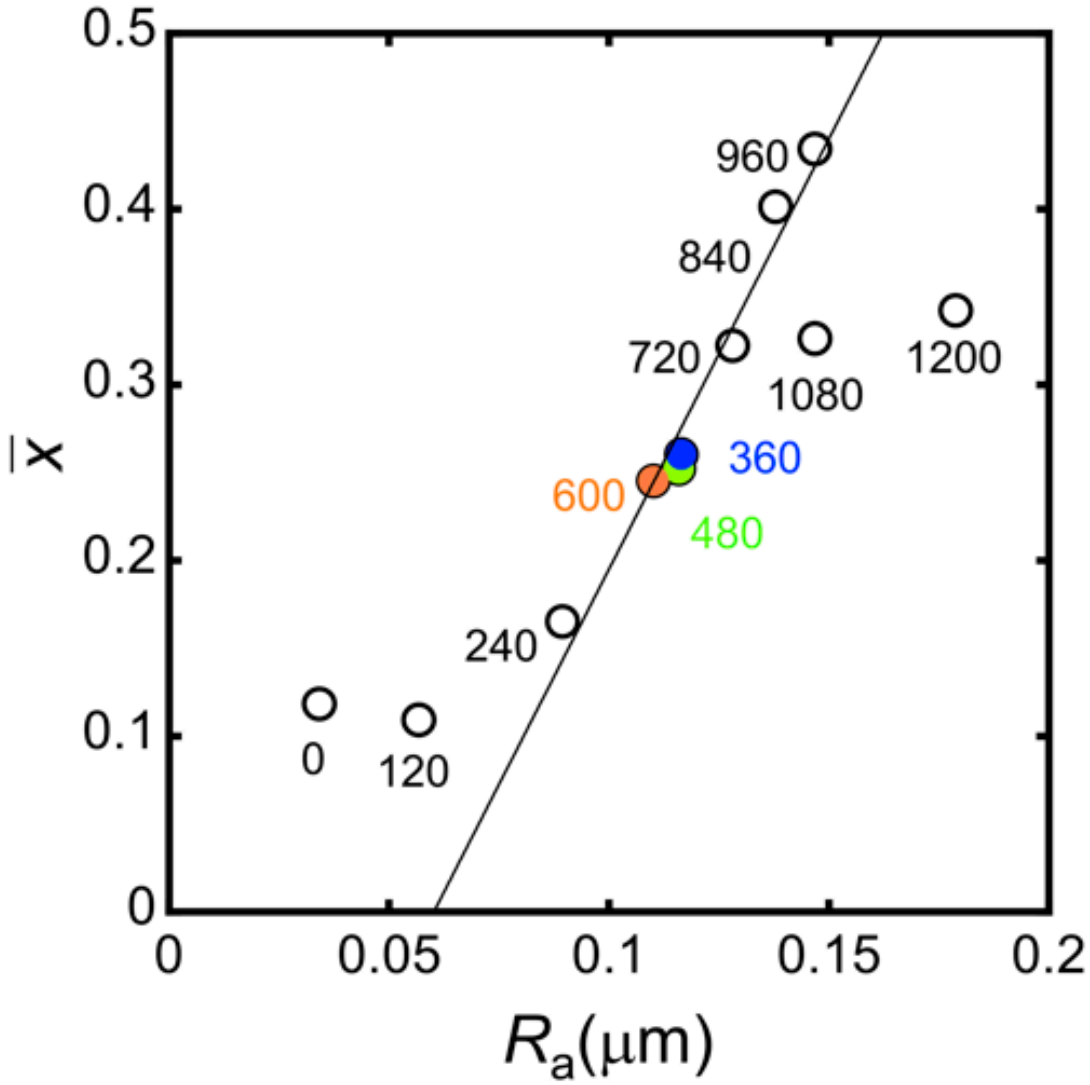

Figure 7 Correlation between surface roughness (R_a) and the average of the friction coefficient ($\bar{x}$). The numbers attached to the markers denote the UV irradiation time in hour. The solid line represents the fitting curve to data from 240 to 960 h.

(A)

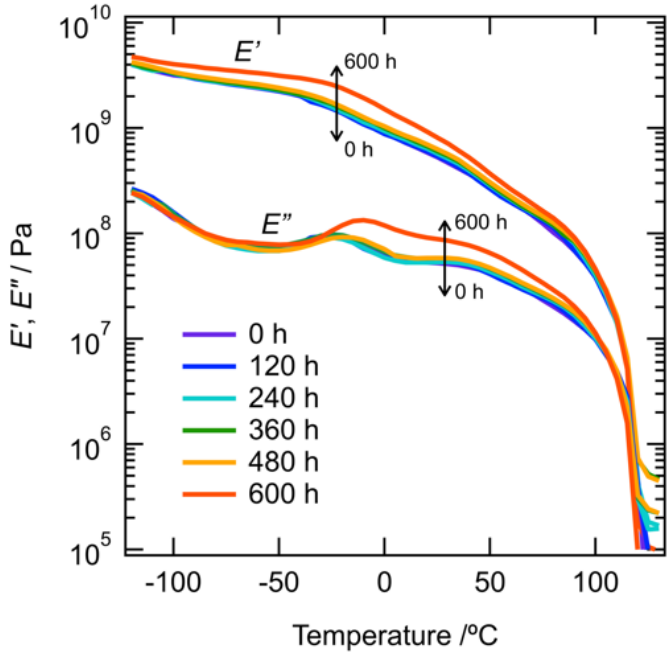

(B)

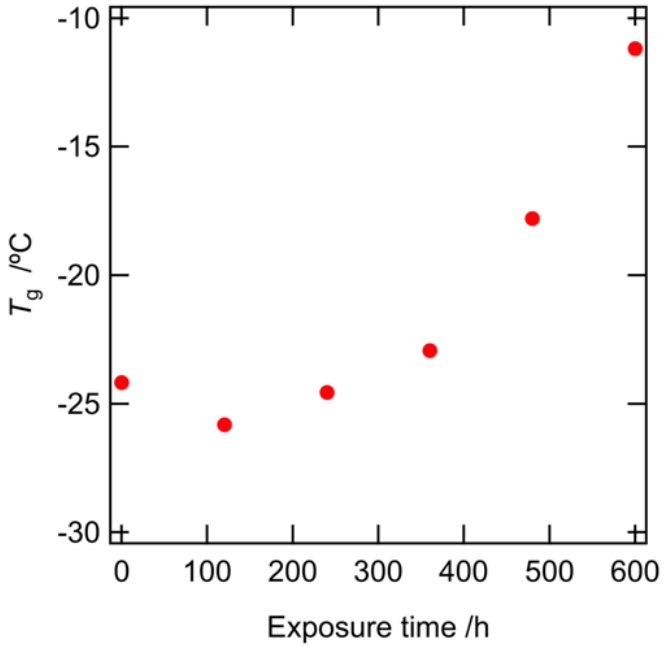

Figure 8 (A) Dynamical mechanical spectra of LDPE specimens at various irradiation times and (B) irradiation time dependence of the glass transition temperature (T_g).

(A)

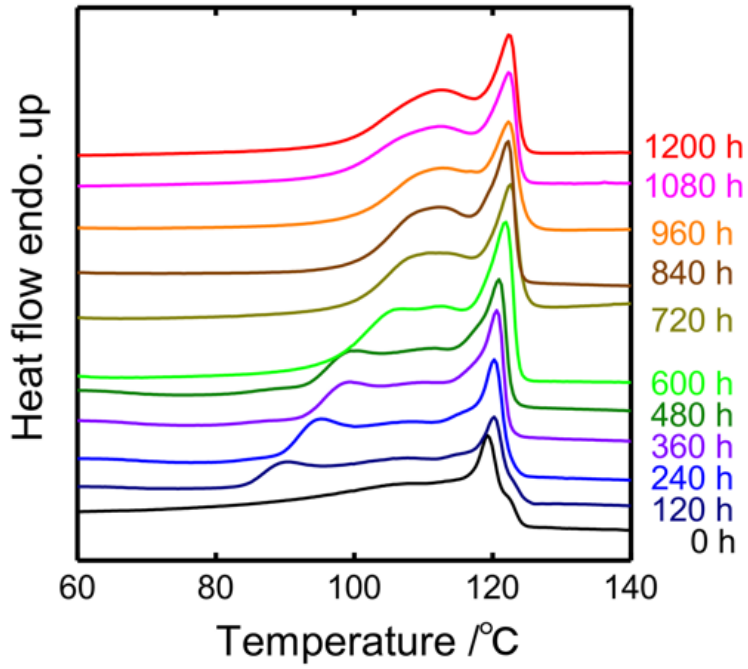

(B)

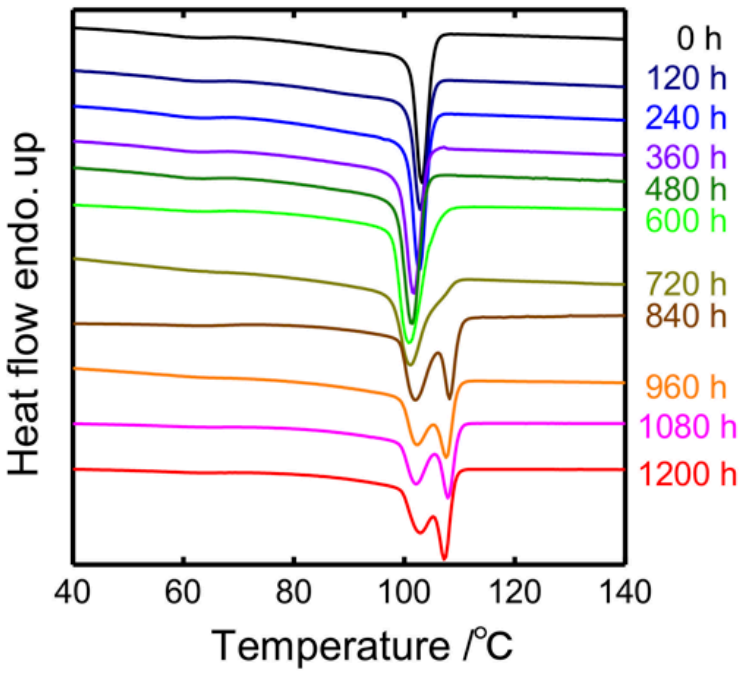

Figure 9 The DSC traces of photodegraded LDPE during (A) heating and (B) cooling. The UV exposure times are shown in the figures.

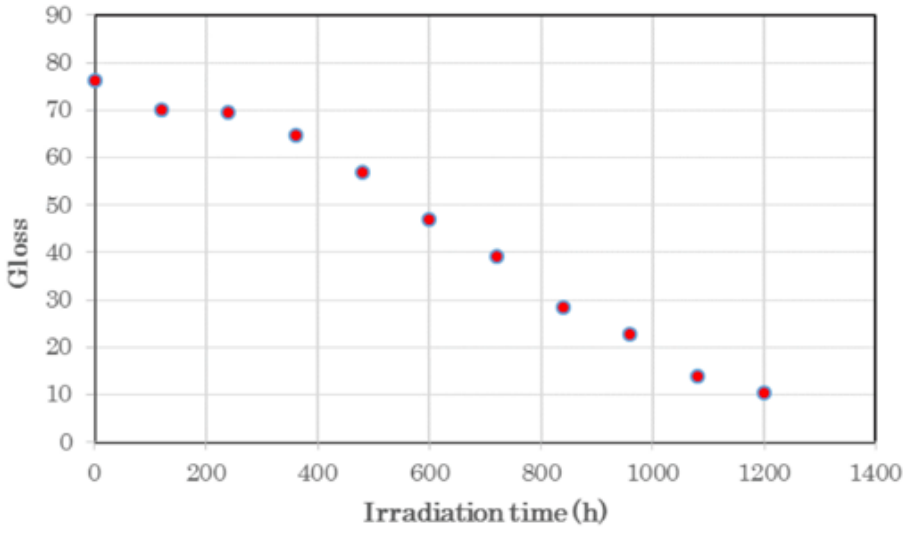

Figure 10 Irradiation time dependence of the gloss of photodegraded LDPE specimens.